

# Tuning electronic and magnetic properties of FeRh alloy by chemical and physical method

Greeshma R and Rudra Banerjee\*

*Department of Physics and Nanotechnology, SRM Institute of Science and Technology, Kattankulathur, Tamil Nadu, 603203, India*

The electronic, magnetic, and thermodynamic properties of ordered and chemically disordered FeRh alloy is studied using *ab-initio* methods. The equiatomic Fe<sub>50</sub>Rh<sub>50</sub> composition is reported for both ordered and disordered phases. Chemically disordered Fe<sub>x</sub>Rh<sub>100-x</sub> is reported and the effect of disorder on electronic and magnetic properties is discussed. Further, We have reported the effects of stress and strain in both the order and disorder phases. The result is only for the cubic phase and no distortion has been taken into consideration. This study is motivated by the recent resurgence in FeRh study motivated by the fact that the barocaloric properties can be possible to sustain over the cycle. Hence, we have discussed the properties of Fe<sub>x</sub>Rh<sub>100-x</sub> with chemical disorder and pressure together, to gain an insight into the compound effect and the interplay between them.

## I. INTRODUCTION

The century old Joule-Thomson effect for cooling technology is not only inefficient but also emits environmentally hazardous by-products. In the last decade caloric materials(CM) has been staged as a feasible alternative due to its environment friendly cooling technology and improved efficiency[1]. The caloric materials show significant adiabatic temperature change ( $\Delta T$ ) or isothermal entropy change ( $\Delta S$ ) near phase boundary under the applied magnetic, electric or mechanical field, corresponding to magnetocaloric(MC)[2], electrocaloric(EC) or mechanocaloric(mC) elasto(eC) or barocaloric(BC)) effects[3]. Though the magnetocaloric effect is believed to be observed first in 19th century[4], the field really took off with the observation of ‘giant’ mC[5], MC[6] and EC[7] in 1980s and subsequent decades.

Various CMs, particularly based on Lanthanides(specially, Gd)[8] and transition metal (specially, Mn[9] and Fe) materials have shown impressive caloric properties. The multicaloric materials, where materials can show caloric properties stimulated by one or multiple fields as described above, are rare and far between. While there are theoretical understanding of multicaloric systems[10], experiments are mostly constrained by individual fields[11]. Off-stoichiometric FeRh system is one of the known systems showing inverse-MC(iMC), BC and EC. FeRh shows giant iMC near room temperature[6] at 350K from a first-order antiferromagnetic (AFM) to ferromagnetic (FM) transition. The transition results around 1% volume expansion, leading to the BC property of FeRh[12–15]. FeRh exhibits around  $\Delta S \approx 20JK^{-1}kg^{-1}$  and  $\Delta T \approx 20K$  at 2T, making it an excellent CM. But, FeRh also shows broad hysteresis[13, 16], leading to a degradation of caloric properties over refrigeration cycles. However, Liu *et.al* has shown[17] that it is possible to enhance the property over the cycles. Qiao *et.al*[18] has recently shown the effect of growth on MC properties of FeRh.

This renewed interest in off-stoichiometric FeRh system demands a detailed look into the electronic and magnetic structure of Fe<sub>x</sub>Rh<sub>100-x</sub>, where  $x$  is the percentage of concentration at a site ranging from 49-51, with varying pressure. In this article, we have delineated our systematic study of Fe<sub>x</sub>Rh<sub>100-x</sub>, subject to hydrostatic pressure. We have studied the variation in the electronic structure, magnetic exchange and magnetic transition temperature of FeRh alloy. We carried out the study of this alloy in both FM and AF domain. The study unveiled that the ground state Fe<sub>x</sub>Rh<sub>100-x</sub> system is ferromagnetic in nature(Fig. (1c)). Hence, in this report, we have focused the complete study on FM behaviour of Fe<sub>x</sub>Rh<sub>100-x</sub>.

## II. METHODS

The off-stoichiometric composition and disordered alloy system is best managed using multiple scattering Green’s function and Coherent Potential Approximation (CPA) respectively. The electronic and magnetic calculations in this study are performed using SPRKKR code[19, 20]. The Perdew, Burke and Ernzerhoff(PBE) generalized gradient approximation (PBE-GGA) is used for exchange-correlational functional[21]. We performed first Brillouin zone

---

\* bnrj.rudra@gmail.com

integrations on the 2500 grid of  $k$ -points and the energy convergence criteria had been set to  $10^{-5} Ry$ . The full potential spin polarised scalar relativistic calculations with angular momentum cut-off  $l_{max} = 2$  has been performed.

Initially we determined the lattice parameter with minimum energy for the  $Fe_{50}Rh_{50}$  structure using the following procedure; i) Procured the lattice parameter from materials project database. ii) Computed the scf of the system, by varying lattice parameter ranging from 94% to 106%, similar calculation is done for each lattice parameters. iii) The curve of lattice parameter vs energy is fitted by quadratic polynomial equation. iv) The minimum of the curve is the optimised lattice parameter. For off-stoichiometric structures, we took the optimised lattice parameter from the stoichiometric calculations as the starting point and followed the steps mentioned above. The optimisation curve of ordered  $Fe_{50}Rh_{50}$  is shown in the Fig. (1b).

The magnetic exchange energy ( $\mathcal{J}_{ij}$ ) was evaluated to understand the effects of magnetic interactions using the Lichtenstein formula[22, 23].

$$\begin{aligned} \mathcal{J}_{ij} &= \frac{1}{4\pi} \int d\varepsilon f(\beta(\varepsilon - \varepsilon_F)) ImTr[\hat{\Delta}_i \hat{T}_{\uparrow}^{ij} \hat{\Delta}_j \hat{T}_{\downarrow}^{ji}] \\ &= \frac{1}{4\pi} \int d\varepsilon f(\beta(\varepsilon - \varepsilon_F)) ImTr[\hat{G}_{\uparrow}^+(\varepsilon) \hat{P}_i \hat{G}_{\downarrow}^+(\varepsilon) \hat{P}_j] \end{aligned} \quad (1)$$

where,  $\hat{T}_{\sigma}^{ij}$  is the scattering path operator for sites  $i$  and  $j$ ,  $\hat{\Delta} \equiv \hat{t}_{i\uparrow} - \hat{t}_{j\downarrow}$  is the single site scattering matrix  $\hat{t}_{i\sigma}$  at site  $i$ ,  $f(x) = 1/(e^x + 1)$ ,  $\beta = 1/k_B T$  and  $\varepsilon_F$  is the Fermi energy,  $\hat{G}_{\sigma}^+(\varepsilon)$  is the retarded Green's function of the spin  $\sigma$  in unperturbed state and  $\hat{P}_i \equiv \hat{H}_{i\uparrow} - \hat{H}_{i\downarrow}$  where,  $\hat{H}_{i\sigma}$  is the on-site term of the Hamiltonian for spin  $\sigma$  at site  $i$ . The  $\mathcal{J}_{ij}$  is reckoned by the energy difference due to the infinitesimal change in magnetic direction, as mapped out from Eqn(1). Finally, the Curie temperature is computed using Mean Field Theory(MFT):

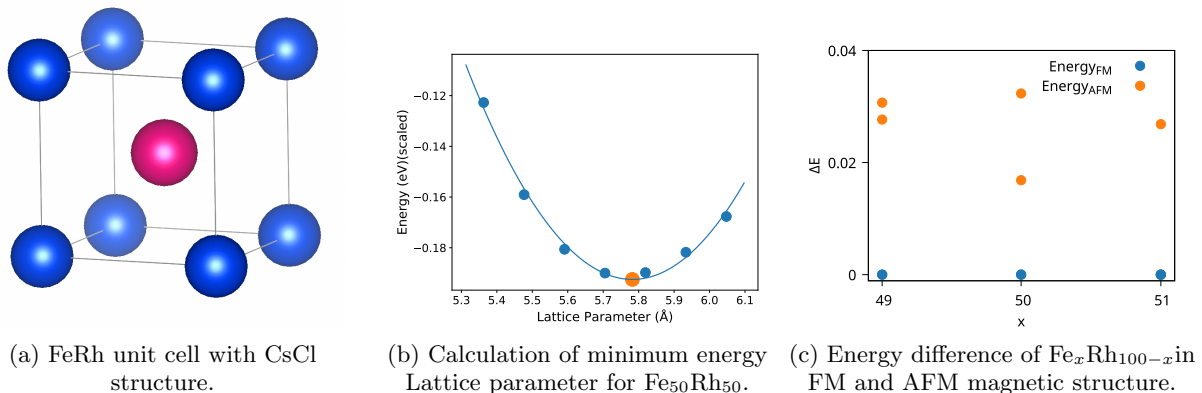


FIG. 1: Initial information of  $Fe_xRh_{100-x}$ . (a) shows the  $Fe_xRh_{100-x}$  structure. In ordered structure Fe and Rh occupies either corner (0,0,0) or central (.5,.5,.5) site. In disordered systems both (0,0,0) and (.5,.5,.5) sites are occupied by Fe and Rh as per concentration. (b) shows the energy minimisation of lattice structure to find the ground state lattice parameter. (c) shows the energy difference between AFM and FM state. In the  $y$ -axis,  $\Delta E = E_{mag} - E_{FM}$  is plotted, where  $E_{mag}$  is either  $E_{FM}$  or  $E_{AFM}$ .

$$k_B T_C = \frac{2}{3} \mathcal{J}_{ij} \quad (2)$$

where,  $\mathcal{J}_{ij}$  is the largest eigen value of the determinant[24, 25].

### III. RESULT

FeRh has CsCl structure in ordered phase(B2-phase), with space group 221 ( $Pm\bar{3}m$ ), as shown in Fig. (1a). In the ordered phase, Fe and Rh occupies (0, 0, 0) and  $(\frac{1}{2}, \frac{1}{2}, \frac{1}{2})$  sublattice, respectively. In chemically disordered phase,  $Fe_{50}Rh_{50}$  stabilises in bcc-A2 structure[25]. In this phase, both Fe and Rh is occupying both sublattices with equal probability.  $Fe_{51}Rh_{49}$  and  $Fe_{49}Rh_{51}$  systems are also disordered with (0,0,0) site is Fe rich or deficient, respectively, as described in Fig. (1a).

## A. Ordered FeRh system

### 1. Electronic Structure

The total and atoms-projected density of states (DOS) for this system is shown in the Fig. (2). Fig. (2b) shows the DOS of  $\text{Fe}_{50}\text{Rh}_{50}$  at optimised lattice parameter. Fig. (2a) is DOS of  $\text{Fe}_{50}\text{Rh}_{50}$  with 6% compressed lattice parameter,

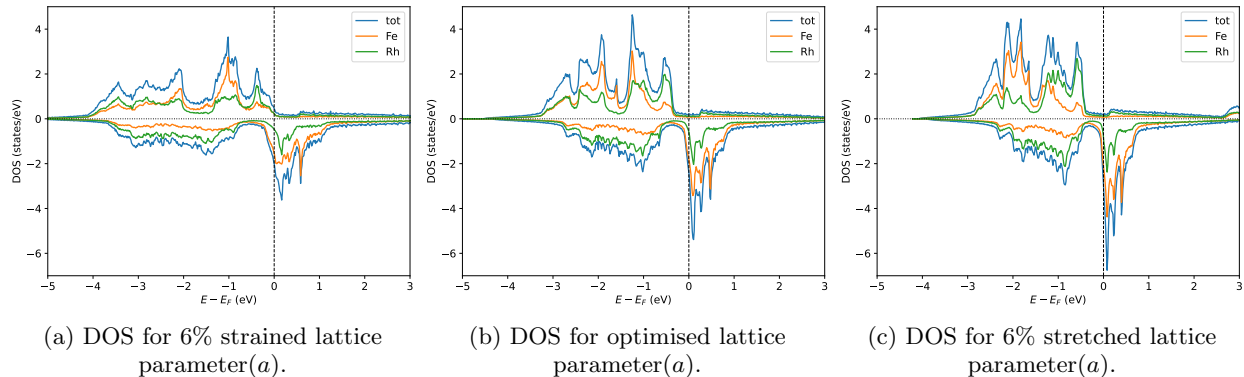


FIG. 2: The electronic structure of ordered  $\text{Fe}_{50}\text{Rh}_{50}$ .

resembling very high hydrostatic pressure. Likewise, Fig. (2c) shows the electronic structure of  $\text{Fe}_{50}\text{Rh}_{50}$  with 6% stretch.

The Fig. (2) shows the DOS of  $\text{Fe}_{50}\text{Rh}_{50}$  with (a)strained, (b)optimised and (c)stretched lattice parameter. The pseudogap around 1eV down in minority spin channel in optimised lattice structure is originated from the  $3d$  hybridisation of Fe and Rh. The peak just below the  $E_F$  in Fig. (2a) in the majority spin channel, originating from the hybridisation of the same orbitals shows the Jahn-Teller instability[26, 27]. With the increase in lattice parameter  $a$ , the peak moves further down from  $E_F$ , stabilising against the possible Jahn-Teller distortion. The volume-preserving stretch/strain with varying  $c/a$  ratio may show the enhancement of Jahn-Teller distortion, but the possibility within cubic phase decreases with increase in  $a$ .

In real systems, such a high hydrostatic pressure or stretch is not only nonphysical, but may have other unforeseen effects as well. Here we have used this to check the extreme conditions. In all the following discussions, this 6% stretch/strain has been considered without further explanation.

### 2. Magnetic Properties

Element resolved magnetic moments  $\mu_{Fe}$ ,  $\mu_{Rh}$  and  $\mu_{FeRh}$  of ordered  $\text{Fe}_{50}\text{Rh}_{50}$  is shown in Table (I). For optimised and strained structure,  $\mu_{Fe} > 3\mu_B$  as already noted by previous study[28]. Fig. (3) shows the magnetic interactions

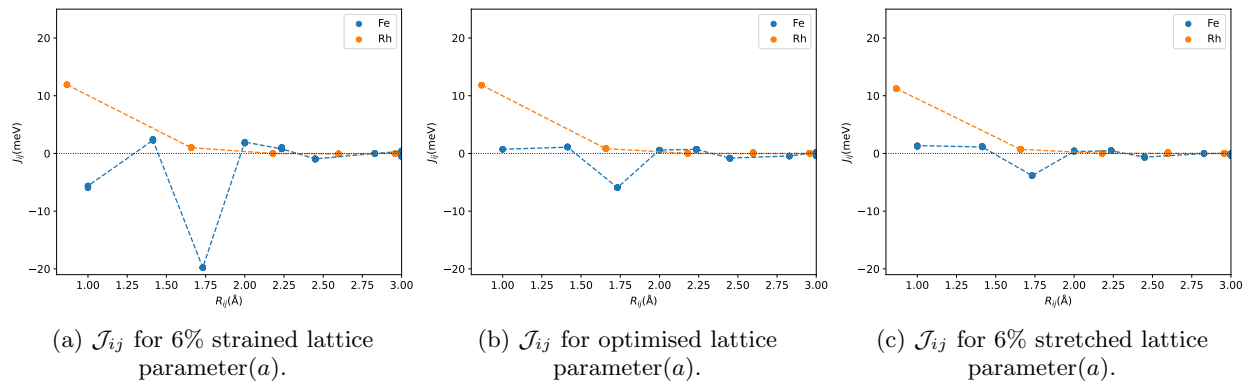


FIG. 3: Magnetic interaction ( $\mathcal{J}_{ij}$ ) of ordered  $\text{Fe}_{50}\text{Rh}_{50}$ .

of ordered  $\text{Fe}_{50}\text{Rh}_{50}$  with Fe of (0,0,0) sublattice at the center. The stretched configuration in Fig. (3a) is interesting

as it is showing very strong alternating positive and negative interaction, leading to a spin-glass like configuration. The glassy phase in FeRh is already known for metastable fcc phase[29–31], but to the best of our knowledge, we are the first to observe spin-glass effect in these 221 systems using pressure only. In optimised or stretched system, the glassy behaviour is not observed, and dominant interactions are ferromagnetic.

## B. Disordered FeRh system

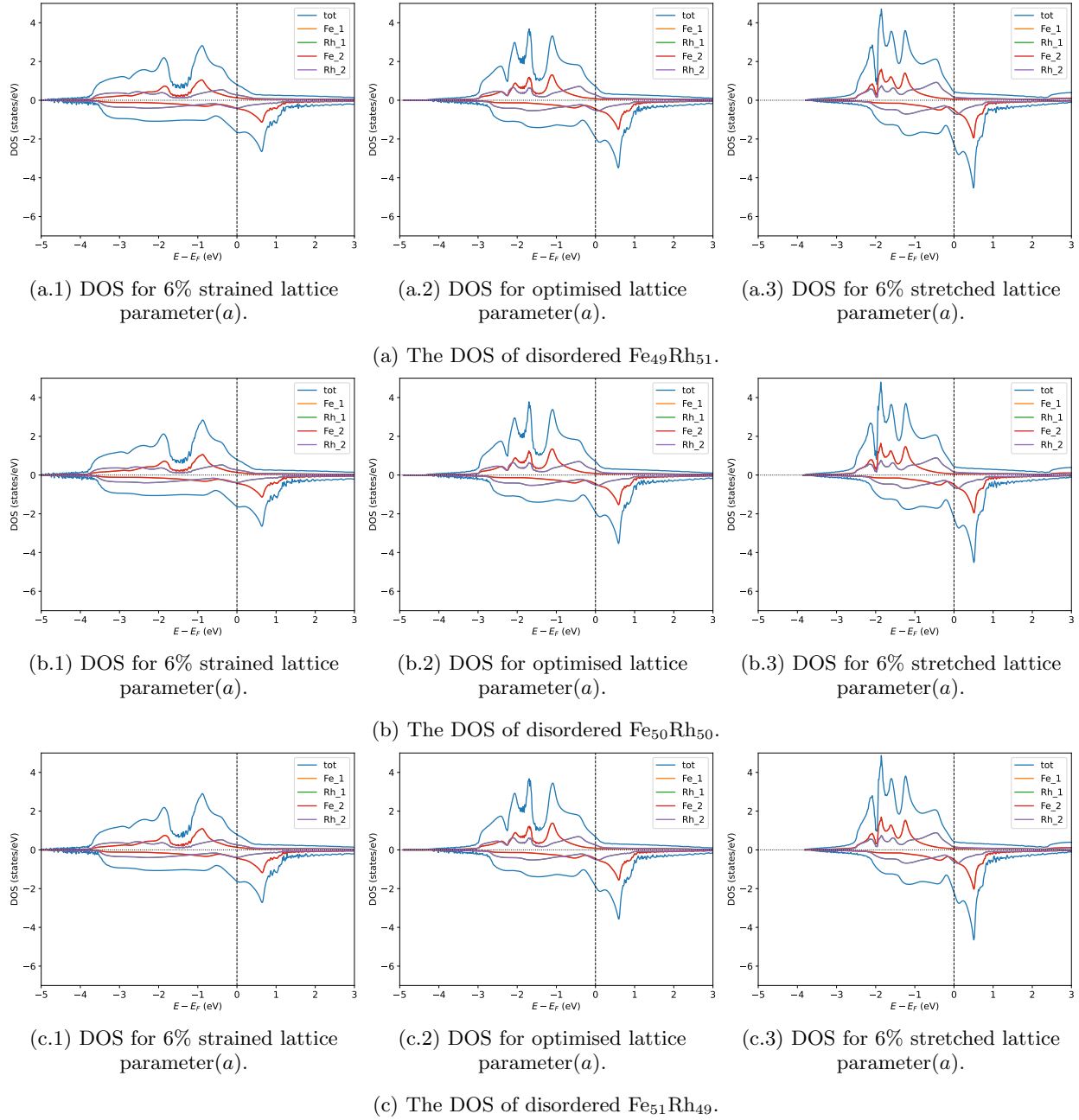


FIG. 4: Electronic structure of disordered  $\text{Fe}_x\text{Rh}_{100-x}$  systems for (a) $x=49$ ,(b)50, and (c)51. While the electronic structures does not change significantly with  $x$ , it does changes with lattice parameter  $a$ : (a) The width of the DOS squeezes with increasing  $a$ . (b) The spin-splitting in atom resolved DOS increases with  $a$ .

In disordered systems  $\text{Fe}_{50}\text{Rh}_{50}$  shows bcc-A2 structure. In this case, Fe and Rh occupies both  $(0,0,0)$  and  $(.5,.5,.5)$  sites with probability according to their concentrations. For brevity, we will denote Fe/Rh at  $(0,0,0)$  as  $\text{Fe}_1/\text{Rh}_1$  and

Fe/Rh at (.5,.5,.5) as Fe<sub>2</sub>/Rh<sub>2</sub>. It has to be noted that in this phase, there are 4 atoms in unit cell, unlike 2 atoms in section (III A)

### 1. Electronic structure

The DOS for disordered phases are shown in the Fig. (4). The DOS is much smeared w.r.t. the ordered DOS plotted in Fig. (2), which is a characteristic of disordered systems[28, 32]. Still, the main features of ordered state is still visible in disordered state as well. The valley near the -2eV in upspin channel is the only distinct feature in strained state. The Rh DOS does not change significantly over the lattice parameter ranges studied, the Fe atom starts showing more and more structures, bringing more features in total DOS. Beside the deep valley, there is also a saddle neck just below the  $E_F$  in major spin channel gets more and more visible. Likewise, the pseudo-gap discussed in the section (III A 1) appears in both optimised and strained state.

### 2. Magnetic Properties

Similar to the electronic structures, magnetic interactions with Fe atom at the center does not change much with concentrations. Unlike the ordered phase in section (III A 2), there is no visible spin glass phase in disordered phase. The variation in magnetic moments of Fe<sub>x</sub>Rh<sub>100-x</sub> and Fe atoms are shown in Fig. (6a) and Fig. (6b). The values are tabulated in last three rows of the table (I). While the moment of Fe is very close to their atomic level (2.412  $\mu_B$  in 221 structure[33]), the moment increases monotonously with the lattice parameter. This trend shows magnetic properties are more dependent on the distance between the atoms rather than the concentrations in this off-stoichiometric systems. The magnetic moment of both Fe and Rh increase with the lattice parameter. This is due to the increased spin-polarisation in both Fe and Rh, as seen in atom projected DOS in Fig. (4). This behaviour is completely different from volume-preserved distortion, where  $\mu_{Rh}$ ,  $\mu_{Fe}$ ,  $\mathcal{J}_0^{Rh}$  and  $\mathcal{J}_0^{Fe}$  decreases lattice parameter[25]. This indicates an establishment of long-range Fe-Fe FM interaction in this case, instead of a competing short-range FM and long-range AFM interactions between Fe.

The Curie temperature calculated using MFT(Eqn(2)) is tabulated in the table (I) and Fig. (6c). Decreasing the Fe content also decreases the  $T_C$ . Our MFT result for B2-Fe<sub>50</sub>Rh<sub>50</sub> matches earlier results obtained using same method. The lattice parameter effects  $T_C$  profoundly, with around 70% increase in  $T_C$  for 12% change in lattice parameter. The higher magnetic splitting in Rh has increased the inter-sublattice interaction, leading to this high  $\mathcal{J}_{ij}$ , leading to the higher  $T_C$ .

Fe	Rh		Magnetic moment ( $\mu_B$ )			$T_C(K)$
			Fe	Rh	FeRh	
50o	50	Stretched	2.9317	0.9319	3.8636	539
	50	Optimised	3.2711	0.9417	4.2128	820
	50	Strained	3.3929	0.9340	4.3269	832
49	51	Stretched	2.7786	0.4301	3.1616	522
	51	Optimised	3.0774	0.7173	3.7475	772
	51	Strained	3.2200	0.9620	4.1369	907
50d	50	Stretched	2.7472	0.4239	3.1711	527
	50	Optimised	3.0703	0.7253	3.7956	760
	50	Strained	3.2062	0.9480	4.1542	908
51	49	Stretched	2.7679	0.4494	3.2637	546
	49	Optimised	3.0631	0.7331	3.8427	784
	49	Strained	3.2058	0.9531	4.2042	912

TABLE I: Magnetic properties of Fe<sub>x</sub>Rh<sub>100-x</sub>. The 50o and 50d in first and third row means the results are for ordered and disordered Fe<sub>50</sub>Rh<sub>50</sub>.

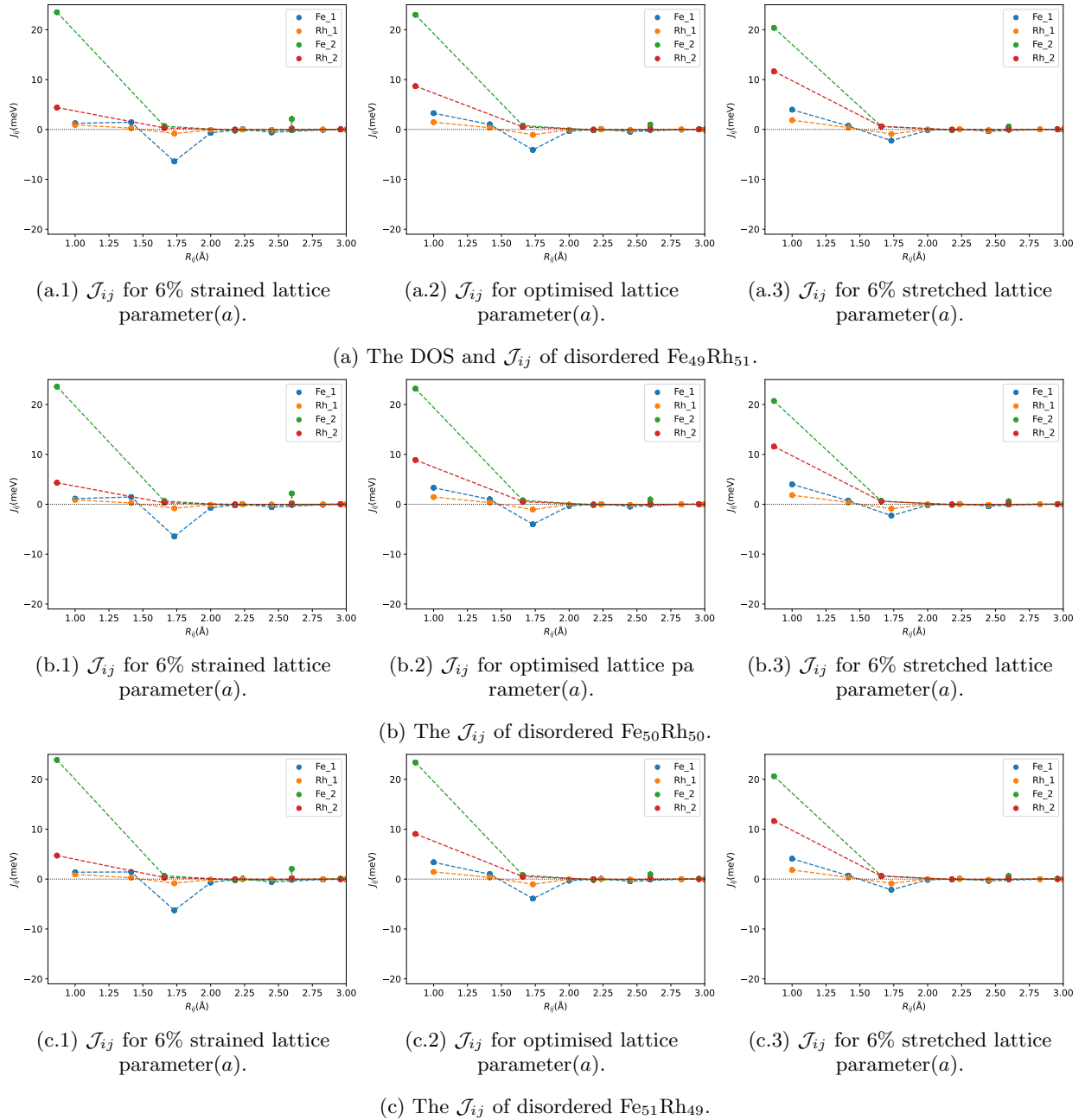


FIG. 5:  $\mathcal{J}_{ij}$  of disordered  $\text{Fe}_x\text{Rh}_{100-x}$  systems for (a)  $x = 49$ , (b) 50 and (c) 51 with  $\text{Fe}_1$  at the center. Similar to the electronic structures, magnetic exchange interactions is not much changed with variations in  $x$ . The stress/strain, i.e. variation in  $a$  changes the  $\mathcal{J}_{ij}$  significantly. The  $\mathcal{J}_0^{Fe}$  decreases slightly with increasing  $a$ , but  $\mathcal{J}_0^{Rh}$  has increased to almost double with 12% change in  $a$ .

#### IV. CONCLUSION

In this communication, we have presented, electronic and magnetic properties of  $\text{Fe}_x\text{Rh}_{100-x}$  as obtained from density functional theory based calculations. The main outcome of the calculations can be summarised as (i) The electronic structures of  $\text{Fe}_x\text{Rh}_{100-x}$  matches well with previous calculations. (ii) The magnetic moment of both Fe and Rh is higher than the free atoms. The magnetic moment of Rh in disordered phase is due to the hybridisation of nearest neighbour Fe. (iii) Both electronic and magnetic properties has stronger dependency on the distance between nearest neighbours or the lattice parameters than the small variations in composition. Particularly, we have shown the effect of chemical disorder and pressure on electronic and magnetic properties of  $\text{Fe}_x\text{Rh}_{100-x}$  both separately and

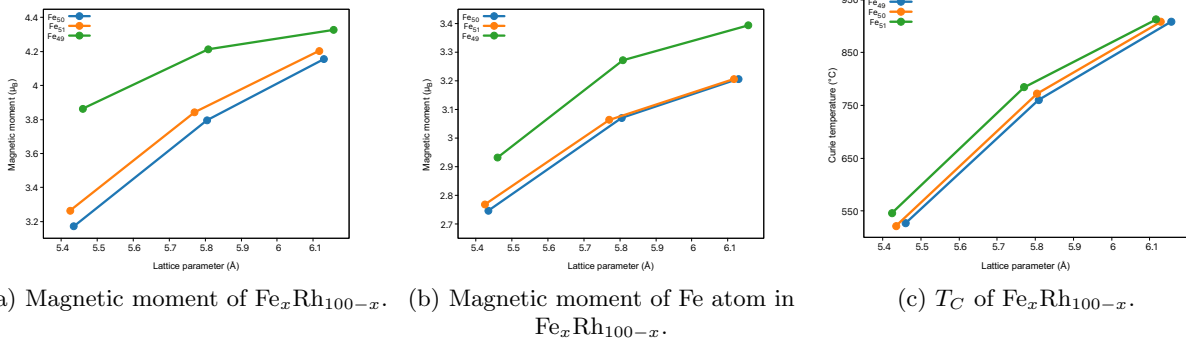


FIG. 6: Variation of Magnetic moment and Curie temperature of ordered Fe<sub>x</sub>Rh<sub>100-x</sub> with  $x$  and  $a$ .

together. This will help further understanding and designing Fe-based caloric materials.

## V. ACKNOWLEDGMENT

We acknowledge the High Performance Computing Center (HPCC), SRM IST for providing the computational facility to carry out this research work successfully.

- 
- [1] L. J. Swartzendruber. The fe-rh (iron-rhodium) system. *Bulletin of Alloy Phase Diagrams*, 5(5):456–462, oct 1984.
  - [2] J. B. Staunton, R. Banerjee, M. dos Santos Dias, A. Deak, and L. Szunyogh. Fluctuating local moments, itinerant electrons, and the magnetocaloric effect: Compositional hypersensitivity of FeRh. *Physical Review B*, 89(5), feb 2014.
  - [3] X. Moya, S. Kar-Narayan, and N. D. Mathur. Caloric materials near ferroic phase transitions. *Nature Materials*, 13(5):439–450, apr 2014.
  - [4] Anders Smith. Who discovered the magnetocaloric effect? *The European Physical Journal H*, 38(4):507–517, jun 2013.
  - [5] C. Rodriguez and L. C. Brown. The thermal effect due to stress-induced martensite formation in  $\beta$ -CuAlNi single crystals. *Metallurgical Transactions A*, 11(1):147–150, dec 1980.
  - [6] S.A. Nikitin, G. Myaligulyev, A.M. Tishin, M.P. Annaorazov, K.A. Asatryan, and A.L. Tyurin. The magnetocaloric effect in fe49rh51 compound. *Physics Letters A*, 148(6-7):363–366, aug 1990.
  - [7] A. S. Mischenko, Q. Zhang, J. F. Scott, R. W. Whatmore, and N. D. Mathur. Giant electrocaloric effect in thin-film PbZr<sub>0.95</sub>Ti<sub>0.05</sub>O<sub>3</sub>. *Science*, 311(5765):1270–1271, mar 2006.
  - [8] A. Fujita, S. Fujieda, Y. Hasegawa, and K. Fukamichi. Itinerant-electron metamagnetic transition and large magnetocaloric effects in La(fe<sub>x</sub>si<sub>1-x</sub>)<sub>13</sub> compounds and their hydrides. *Physical Review B*, 67(10), mar 2003.
  - [9] Nguyen H. Dung, Zhi Qiang Ou, Luana Caron, Lian Zhang, Dinh T. Cam Thanh, Gilles A. de Wijs, Rob A. de Groot, K. H. Jürgen Buschow, and Ekkes Brück. Mixed magnetism for refrigeration and energy conversion. *Advanced Energy Materials*, 1(6):1215–1219, sep 2011.
  - [10] Yang Liu, Ingrid C Infante, Xiaojie Lou, Laurent Bellaiche, James F Scott, and Brahim Dkhil. Giant room-temperature elastocaloric effect in ferroelectric ultrathin films. *Advanced Materials*, 26(35):6132–6137, 2014.
  - [11] J Krishna Murthy and A Venimadhav. Multicaloric effect in multiferroic y2csmno6. *Journal of Physics D: Applied Physics*, 47(44):445002, 2014.
  - [12] Enric Stern-Taulats, Antoni Planes, Pol Lloveras, Maria Barrio, Josep-Lluís Tamarit, Sabyasachi Pramanick, Subham Majumdar, Carlos Frontera, and Lluís Mañosa. Barocaloric and magnetocaloric effects in Fe<sub>49</sub>Rh<sub>51</sub>. *Physical Review B*, 89(21), jun 2014.
  - [13] Enric Stern-Taulats, Adrià Gràcia-Condal, Antoni Planes, Pol Lloveras, Maria Barrio, Josep-Lluís Tamarit, Sabyasachi Pramanick, Subham Majumdar, and Lluís Mañosa. Reversible adiabatic temperature changes at the magnetocaloric and barocaloric effects in fe49rh51. *Applied Physics Letters*, 107(15):152409, 2015.
  - [14] V. L. Moruzzi and P. M. Marcus. Antiferromagnetic-ferromagnetic transition in ferh. *Phys. Rev. B*, 46(0):2864–2873, Aug 1992.
  - [15] Enric Stern-Taulats, Antoni Planes, Pol Lloveras, Maria Barrio, Josep-Lluís Tamarit, Sabyasachi Pramanick, Subham Majumdar, Carlos Frontera, and Lluís Mañosa. Barocaloric and magnetocaloric effects in fe49rh51. *Phys. Rev. B*, 89(8):214105, Jun 2014.
  - [16] V Franco, JS Blázquez, B Ingale, and A Conde. The magnetocaloric effect and magnetic refrigeration near room temperature: materials and models. *Annual Review of Materials Research*, 42:305–342, 2012.

- [17] Yang Liu, Lee C. Phillips, Richard Mattana, Manuel Bibes, Agnès Barthélémy, and Brahim Dkhil. Large reversible caloric effect in FeRh thin films via a dual-stimulus multicaloric cycle. *Nature Communications*, 7(1), may 2016.
- [18] Kaiming Qiao, Yuhang Liang, Hu Zhang, Fengxia Hu, Ziyuan Yu, Yi Long, Jing Wang, Jirong Sun, Tongyun Zhao, and Baogen Shen. Manipulation of magnetocaloric effect in FeRh films by epitaxial growth. *Journal of Alloys and Compounds*, 907:164574, jun 2022.
- [19] H Ebert and et.al. The munich spr-krk package.
- [20] H Ebert, D Ködderitzsch, and J Minár. Calculating condensed matter properties using the KKR-green's function method—recent developments and applications. *Reports on Progress in Physics*, 74(9):096501, aug 2011.
- [21] John P. Perdew, Kieron Burke, and Matthias Ernzerhof. Generalized gradient approximation made simple. *Phys. Rev. Lett.*, 77:3865–3868, Oct 1996.
- [22] A I Liechtenstein, M I Katsnelson, and V A Gubanov. Exchange interactions and spin-wave stiffness in ferromagnetic metals. *Journal of Physics F: Metal Physics*, 14(7):L125–L128, jul 1984.
- [23] Asako Terasawa, Munehisa Matsumoto, Taisuke Ozaki, and Yoshihiro Gohda. Efficient algorithm based on liechtenstein method for computing exchange coupling constants using localized basis set. *Journal of the Physical Society of Japan*, 88(11):114706, nov 2019.
- [24] A.I. Liechtenstein, M.I. Katsnelson, V.P. Antropov, and V.A. Gubanov. Local spin density functional approach to the theory of exchange interactions in ferromagnetic metals and alloys. *Journal of Magnetism and Magnetic Materials*, 67(1):65–74, may 1987.
- [25] Ralf Witte, Robert Kruk, Markus E. Gruner, Richard A. Brand, Di Wang, Sabine Schlabach, Andre Beck, Virgil Provenzano, Rossitza Pentcheva, Heiko Wende, and Horst Hahn. Tailoring magnetic frustration in strained epitaxial FeRh films. *Physical Review B*, 93(10), mar 2016.
- [26] Tufan Roy, Dhanshree Pandey, and Aparna Chakrabarti. Probing the possibility of coexistence of martensite transition and half-metallicity in ni and co-based full-heusler alloys: *Anabinitiocalculation*. *Physical Review B*, 93(18), may 2016.
- [27] C. Bordel, J. Juraszek, David W. Cooke, C. Baldasseroni, S. Mankovsky, J. Minár, H. Ebert, S. Moyerman, E. E. Fullerton, and F. Hellman. Fe spin reorientation across the metamagnetic transition in strained ferh thin films. *Phys. Rev. Lett.*, 109:117201, Sep 2012.
- [28] J. Kudrnovský, V. Drchal, and I. Turek. Physical properties of FeRh alloys: The antiferromagnetic to ferromagnetic transition. *Physical Review B*, 91(1), jan 2015.
- [29] E Navarro, M Multigner, A. R Yavari, and A Hernando. The spin glass state of metastable fcc FeRh. *Europhysics Letters (EPL)*, 35(4):307–312, aug 1996.
- [30] Jiahui Chen, Ya Gao, Liang Wu, Jing Ma, and Ce-Wen Nan. A magnetic glass state over the first-order ferromagnetic-to-antiferromagnetic transition in FeRh film. *Materials Research Letters*, 5(5):329–334, feb 2017.
- [31] Radhika Barua, Xiujuan Jiang, Felix Jimenez-Villacorta, J. E. Shield, D. Heiman, and L. H. Lewis. Tuning the magnetostructural phase transition in FeRh nanocomposites. *Journal of Applied Physics*, 113(2):023910, jan 2013.
- [32] Rudra Banerjee and Abhijit Mookerjee. Augmented space recursion code and application in simple binary metallic alloy. *International Journal of Modern Physics C*, 21(02):205–220, feb 2010.
- [33] Materials Project database.